

# Nuclear structure aspects of spin-independent WIMP scattering off xenon

L. Vietze,<sup>1,2,\*</sup> P. Klos,<sup>1,2,†</sup> J. Menéndez,<sup>1,2,‡</sup> W. C. Haxton,<sup>3,4,§</sup> and A. Schwenk<sup>1,2,¶</sup>

<sup>1</sup>*Institut für Kernphysik, Technische Universität Darmstadt, 64289 Darmstadt, Germany*

<sup>2</sup>*ExtreMe Matter Institute EMMI, GSI Helmholtzzentrum für Schwerionenforschung GmbH, 64291 Darmstadt, Germany*

<sup>3</sup>*Department of Physics, University of California, Berkeley, CA 94720, USA*

<sup>4</sup>*Lawrence Berkeley National Laboratory, Berkeley, CA 94720, USA*

We study the structure factors for spin-independent WIMP scattering off xenon based on state-of-the-art large-scale shell-model calculations, which are shown to yield a good spectroscopic description of all experimentally relevant isotopes. Our results are based on the leading scalar one-body currents only. At this level and for the momentum transfers relevant to direct dark matter detection, the structure factors are in very good agreement with the phenomenological Helm form factors used to give experimental limits for WIMP-nucleon cross sections. In contrast to spin-dependent WIMP scattering, the spin-independent channel, at the one-body level, is less sensitive to nuclear structure details. In addition, we explicitly show that the structure factors for inelastic scattering are suppressed by  $\sim 10^{-4}$  compared to the coherent elastic scattering response. This implies that the detection of inelastic scattering will be able to discriminate clearly between spin-independent and spin-dependent scattering. Finally, we provide fits for all calculated structure factors.

PACS numbers: 95.35.+d, 12.39.Fe, 21.60.Cs

## I. INTRODUCTION

About 27% of the energy density in the universe consists of dark matter that rarely interacts with baryonic matter [1]. Weakly interacting massive particles (WIMPs), postulated by supersymmetric extensions of the standard model, are among the most promising dark matter candidates, as their predicted density would naturally account for the observed dark matter density [2]. Furthermore, WIMPs interact with quarks, allowing for direct dark matter detection by the observation of the nuclear recoil induced by WIMP scattering off nuclei [3]. Several experiments worldwide are searching for this dark matter signature [4–9], but so far no unambiguous detection has been achieved. In addition, WIMPs could also scatter inelastically [10], thereby exciting the nucleus and yielding a different dark matter signal.

The analysis of direct detection experiments requires knowledge of the nuclear structure factors. For a given coupling between WIMPs and nucleons, these encode the nuclear structure aspects relevant for WIMP-nucleus scattering. In this work, we calculate the structure factors for spin-independent (SI) WIMP scattering, complementing our previous work on elastic [11, 12] and inelastic [13] spin-dependent (SD) interactions. We focus on scattering off xenon, which is used as target of major direct detection experimental efforts such as XENON and LUX [8, 9].

For the SI WIMP coupling to nucleons, we take the standard scalar-isoscalar current-current interaction Lagrangian as discussed in Ref. [14]. In addition, a reliable description of the nuclear states involved in the scattering process is needed. In this work, we perform state-of-the-art nuclear structure calculations, which take advantage of progress in nuclear interactions and computing capabilities, and compare our results to the phenomenological structure factors typically used in dark matter detection analyses and to other calculations.

This paper is organized as follows. In Sec. II we discuss the structure factor for SI scattering starting from the effective WIMP-nucleon interaction Lagrangian, considering the leading scalar one-body currents. Our nuclear structure calculations are discussed in Sec. III. In Sec. IV we present the resulting structure factors for elastic SI WIMP scattering off all stable xenon isotopes. These are compared in Sec. V to the phenomenological Helm form factors used in most analyses of direct detection experiments. We also compare our results to the recent calculations of Fitzpatrick *et al.* [15], for both SI and SD cases. Inelastic WIMP scattering off xenon and its capability to distinguish between SI and SD interactions are discussed in Sec. VI. Finally, we summarize in Sec. VII.

## II. SPIN-INDEPENDENT WIMP-NUCLEUS SCATTERING

The SI interaction of WIMPs with nuclei, assuming spin 1/2 neutralinos, is described by the low-momentum-transfer Lagrangian [14]

$$\mathcal{L}_\chi^{\text{SI}} = \frac{G_F}{\sqrt{2}} \int d^3\mathbf{r} j(\mathbf{r}) S(\mathbf{r}), \quad (1)$$

where  $G_F$  is the Fermi coupling constant, and  $j(\mathbf{r})$  and  $S(\mathbf{r})$  denote the scalar leptonic and the scalar hadronic

\* E-mail: lvietze@theorie.ikp.physik.tu-darmstadt.de

† E-mail: pklos@theorie.ikp.physik.tu-darmstadt.de

‡ E-mail: menendez@nt.phys.s.u-tokyo.ac.jp;

Present address: Department of Physics, University of Tokyo, Hongo, Tokyo 113-0033, Japan

§ E-mail: haxton@berkeley.edu

¶ E-mail: schwenk@physik.tu-darmstadt.de

current, respectively. The leptonic current is given by kinematics of the WIMP field  $\chi$ ,

$$j(\mathbf{r}) = \bar{\chi}\chi = \delta_{s_f, s_i} e^{-i\mathbf{q}\cdot\mathbf{r}}, \quad (2)$$

where  $s_f, s_i = \pm 1/2$  are the final and initial spin projections of the WIMP and  $\mathbf{q}$  is the momentum transfer from nucleons to neutralinos. As in Ref. [14], we take the hadronic current of the nucleons to be purely isoscalar with coupling  $c_0$ . We take into account only the leading one-body currents, so that the scalar nuclear current is a sum over single nucleons,

$$S(\mathbf{r}) = c_0 \sum_{i=1}^A \delta^{(3)}(\mathbf{r} - \mathbf{r}_i). \quad (3)$$

However, additional contributions enter from two-body currents [16, 17], whose importance is under discussion [18].

The differential cross section for SI WIMP scattering off a nucleus with initial state  $|i\rangle$  and final state  $|f\rangle$  is obtained from the Lagrangian density of Eq. (1) [14]:

$$\begin{aligned} \frac{d\sigma}{dq^2} &= \frac{2}{(2J_i + 1)\pi v^2} \sum_{s_f, s_i} \sum_{M_f, M_i} |\langle f | \mathcal{L}_\chi^{\text{SI}} | i \rangle|^2 \\ &= \frac{8G_F^2}{(2J_i + 1)v^2} S_S(q). \end{aligned} \quad (4)$$

The total angular momentum of the initial and final states of the nucleus are denoted by  $J_i$  and  $J_f$ , with projections  $M_i$  and  $M_f$ ,  $v$  is the WIMP velocity, and  $S_S(q)$  is the scalar structure factor. As the target is unpolarized, one averages over initial projections and sums over the final ones. Following Ref. [19], the structure factor can be decomposed as a sum over multipoles ( $L$ ) of the reduced matrix elements of the Coulomb projection  $\mathcal{C}_L$  of the scalar current:

$$S_S(q) = \sum_{L=0}^{\infty} |\langle J_f | \mathcal{C}_L(q) | J_i \rangle|^2, \quad (5)$$

with

$$\mathcal{C}_{LM}(q) = c_0 \sum_{i=1}^A j_L(qr_i) Y_{LM}(\mathbf{r}_i). \quad (6)$$

Each Coulomb multipole in Eq. (6) has a given parity set by the spherical harmonic,  $\Pi(Y_{LM}) = (-1)^L$ . For elastic scattering the initial and final states are the same and  $J_i^{\Pi_i} = J_f^{\Pi_f}$ , so that only even  $L$  multipoles contribute. For inelastic scattering the parity of the initial and final states can differ, and the allowed multipoles are given by

$$\Pi_f = \Pi_i \Rightarrow L \text{ even}, \quad (7)$$

$$\Pi_f \neq \Pi_i \Rightarrow L \text{ odd}. \quad (8)$$

Note that the odd  $L$  multipoles in elastic scattering are also forbidden by time-reversal symmetry.

### III. SPECTRA OF EVEN-MASS XENON ISOTOPES

Xenon has proton number  $Z = 54$ , and the neutron number of the stable isotopes ranges from  $N = 74 - 82$ . Our calculations assume an isospin symmetric  $^{100}\text{Sn}$  core. For the remaining nucleons we consider a valence space consisting of the  $0g_{7/2}$ ,  $1d_{5/2}$ ,  $1d_{3/2}$ ,  $2s_{1/2}$ , and  $0h_{11/2}$  orbitals, both for neutrons and protons, and the effective nuclear interaction GCN5082 [20, 21]. The same valence space and nuclear interaction have been used for the study of SD WIMP scattering off the odd-mass isotopes  $^{129}\text{Xe}$  and  $^{131}\text{Xe}$  [11–13] and for the neutrinoless double-beta decay of  $^{136}\text{Xe}$  [20, 21]. Throughout all calculations we use the shell-model code ANTOINE [22, 23].

The even-mass isotopes  $^{132}\text{Xe}$ ,  $^{134}\text{Xe}$ , and  $^{136}\text{Xe}$  are calculated by exact diagonalization in the valence space. However, for  $^{128}\text{Xe}$  and  $^{130}\text{Xe}$ , proton and neutron excitations from the  $0g_{7/2}$  and  $1d_{5/2}$  into the  $1d_{3/2}$ ,  $2s_{1/2}$ , and  $0h_{11/2}$  orbitals were restricted to three and six, respectively, to keep the matrix dimension tractable. These truncations should not affect the most important shell-model configurations. The matrix dimensions associated with the nuclear structure calculations of the even-mass xenon isotopes are given in Table I.

Figures 1–5 compare the calculated spectra of the stable even-mass xenon isotopes to experiment. The ten lowest lying states are given. The spectra of  $^{129}\text{Xe}$  and  $^{131}\text{Xe}$  were shown and discussed in Ref. [12]. The overall agreement with experiment is very good in all cases. The spin/parity and location of the first excited  $2_1^+$  state is very well reproduced along the isotopic chain, and the spacing between this state and the following excited states is also in very good agreement with experiment.

In  $^{128}\text{Xe}$ ,  $^{130}\text{Xe}$ , and  $^{132}\text{Xe}$ , the second and third excited states form a doublet of  $2_2^+$ ,  $4_1^+$  states, well separated from other excited states. This situation is well reproduced in our calculations of  $^{130}\text{Xe}$  and  $^{132}\text{Xe}$ , but not for  $^{128}\text{Xe}$ , where the calculated spectra is significantly more compressed than experiment. This disagreement is due to the restrictions imposed on the valence space for the  $^{128}\text{Xe}$  calculations. These truncations mainly affect higher lying states above 1 MeV, so that one can be confident in the calculation of the structure factor for WIMP scattering, as this involves only the ground state.

For  $^{134}\text{Xe}$  and  $^{136}\text{Xe}$ , the second and higher excited states are relatively close to each other (especially in  $^{134}\text{Xe}$ ), and the location and spin/parity of those states

TABLE I. Matrix dimensions for the even-mass xenon isotopes. For  $^{132}\text{Xe}$ ,  $^{134}\text{Xe}$ , and  $^{136}\text{Xe}$  the dimension is that of the full valence space, whereas for  $^{128}\text{Xe}$  and  $^{130}\text{Xe}$  the calculations are restricted (as discussed in the text).

Isotope	$^{128}\text{Xe}$	$^{130}\text{Xe}$	$^{132}\text{Xe}$	$^{134}\text{Xe}$	$^{136}\text{Xe}$
Dimension	$373 \cdot 10^6$	$410 \cdot 10^6$	$21 \cdot 10^6$	$335 \cdot 10^3$	1500

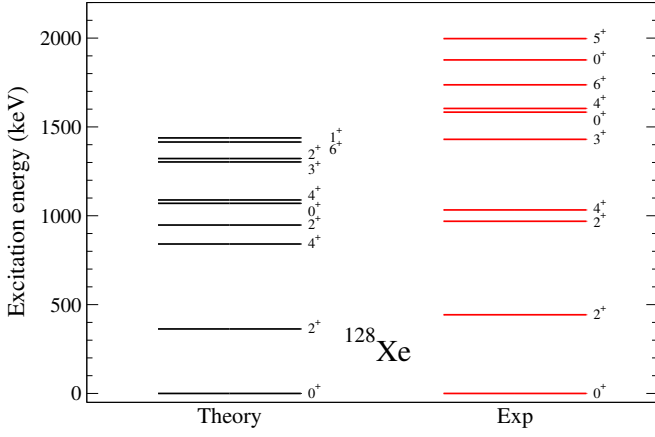


FIG. 1. Comparison of the calculated spectrum of  $^{128}\text{Xe}$  with experiment [24]. The calculation is performed in a restricted valence space (as discussed in the text).

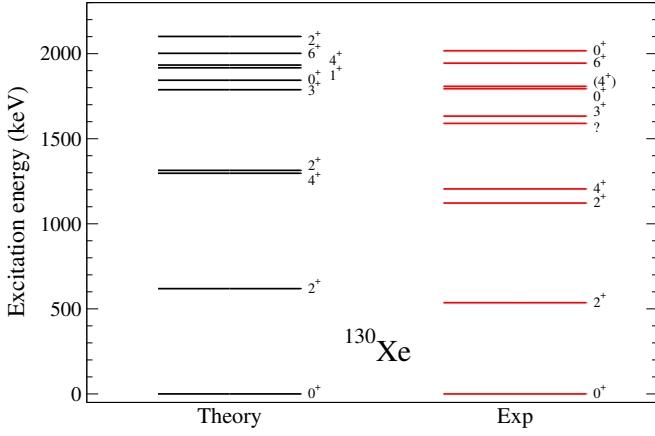


FIG. 2. Comparison of the calculated spectrum of  $^{130}\text{Xe}$  with experiment [24]. The calculation is performed in a restricted valence space (as discussed in the text).

obtained in our calculations in the full valence space is in good agreement to the (sometimes tentative) experimental assignments.

#### IV. STRUCTURE FACTORS FOR SPIN-INDEPENDENT WIMP SCATTERING OFF XENON ISOTOPES

The resulting structure factors for elastic ( $J_i = J_f = J$ ) SI WIMP scattering off the seven stable xenon isotopes are shown in Figs. 6–13. The structure factors  $S_S(q)$  are plotted as a function of the dimensionless variable  $u = q^2 b^2 / 2$ , where  $q$  is the momentum transfer and  $b$  is the harmonic-oscillator length, defined as  $b = \sqrt{\hbar / m\omega}$  with  $m$  the nucleon mass and  $\omega$  the oscillator frequency, taken as  $\hbar\omega = (45A^{-1/2} - 25A^{-2/3})$  MeV.

At zero momentum transfer,  $S_S(0)$  receives contri-

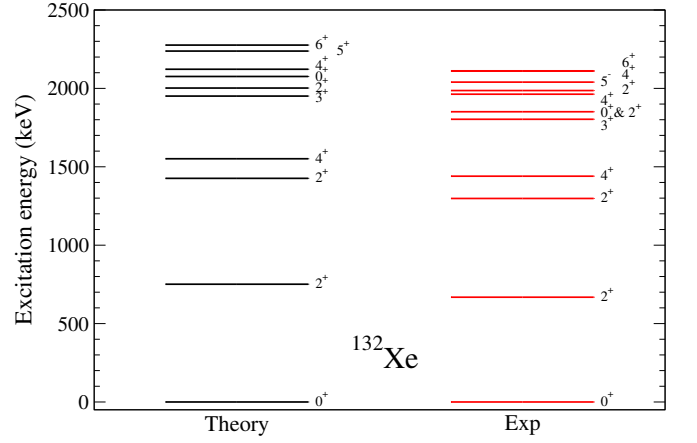


FIG. 3. Comparison of the calculated spectrum of  $^{132}\text{Xe}$  with experiment [24]. The calculation is performed in the full valence space.

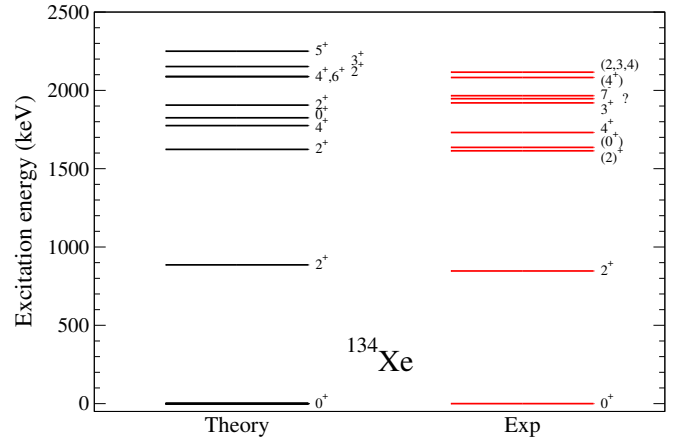


FIG. 4. Same as Fig. 3 but for  $^{134}\text{Xe}$ .

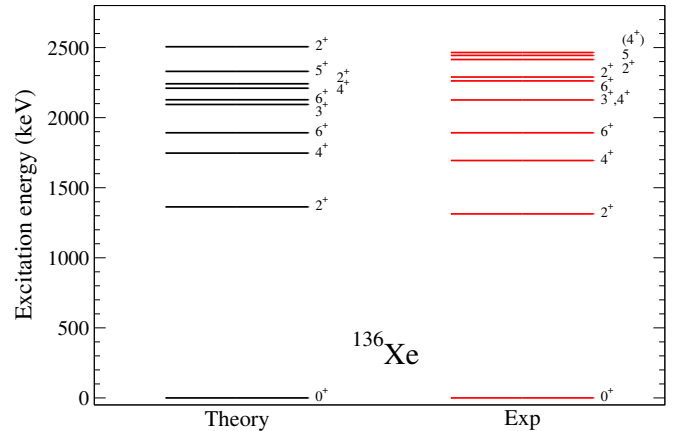


FIG. 5. Same as Fig. 3 but for  $^{136}\text{Xe}$ .

butions only from the  $L = 0$  multipole and is model-

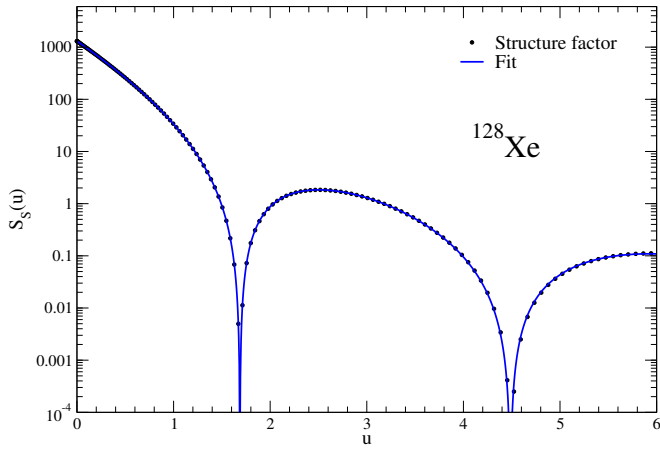


FIG. 6. (color online). Structure factor  $S_S(u)$  for  $^{128}\text{Xe}$  (black dots) with a fit (solid blue line) given in Table II.

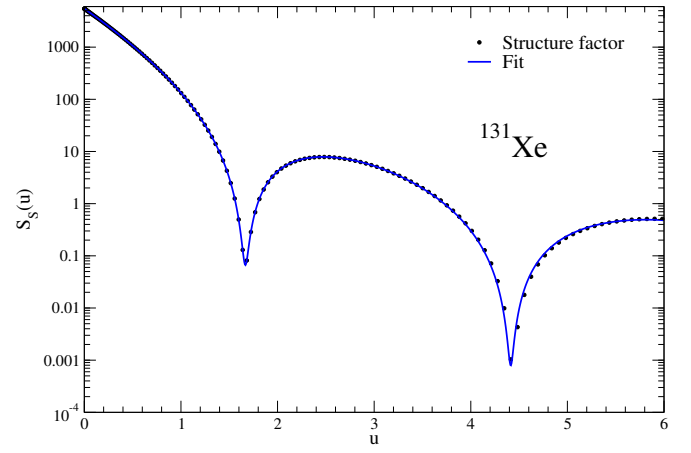


FIG. 9. (color online). Same as Fig. 6 but for  $^{131}\text{Xe}$ .

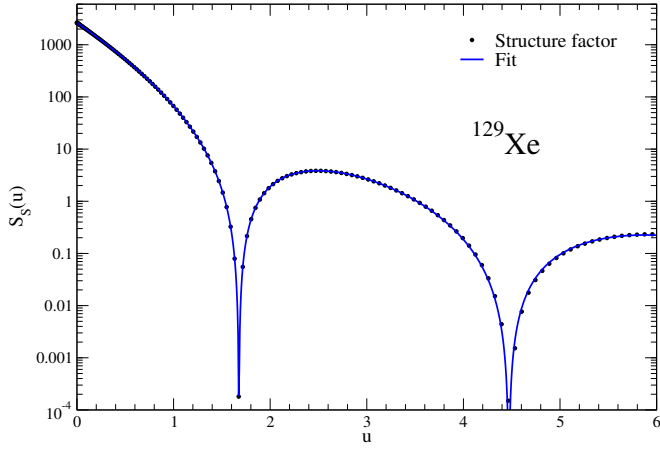


FIG. 7. (color online). Same as Fig. 6 but for  $^{129}\text{Xe}$ .

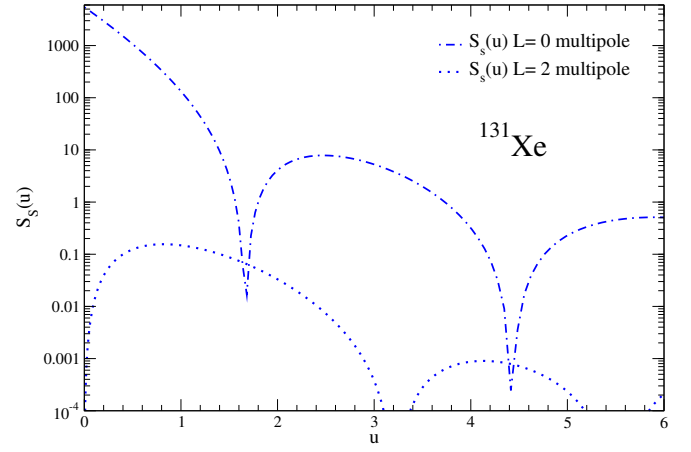


FIG. 10. (color online). Decomposition of the structure factor  $S_S(u)$  for  $^{131}\text{Xe}$  in  $L = 0$  (dashed-dotted line) and  $L = 2$  (dotted line) multipoles.

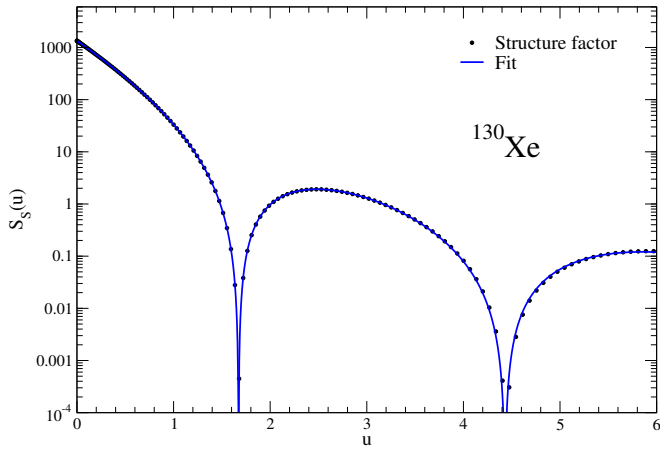


FIG. 8. (color online). Same as Fig. 6 but for  $^{130}\text{Xe}$ .

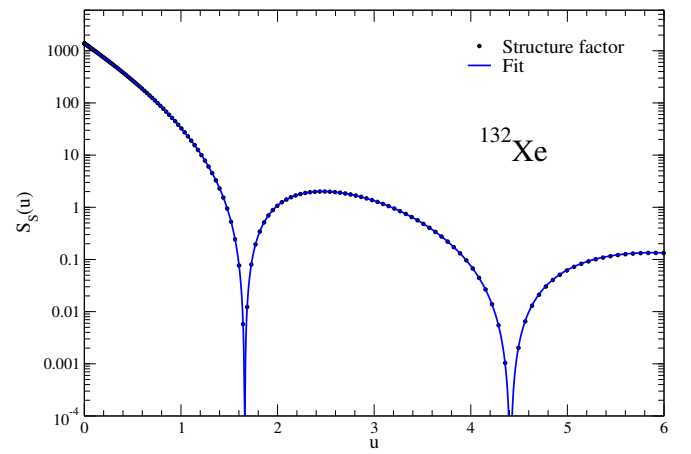


FIG. 11. (color online). Same as Fig. 6 but for  $^{132}\text{Xe}$ .

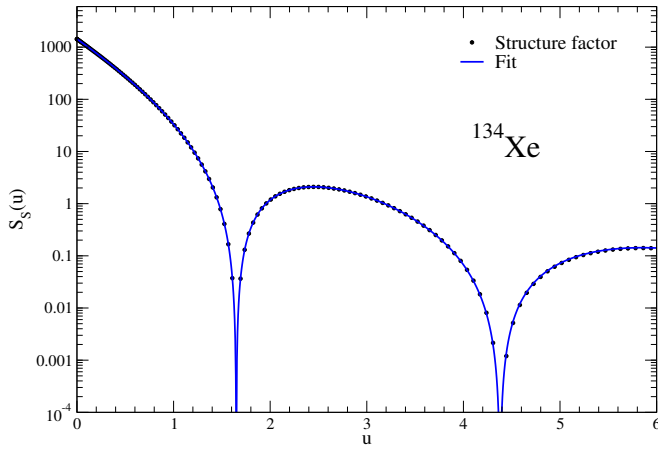


FIG. 12. (color online). Same as Fig. 6 but for  $^{134}\text{Xe}$ .

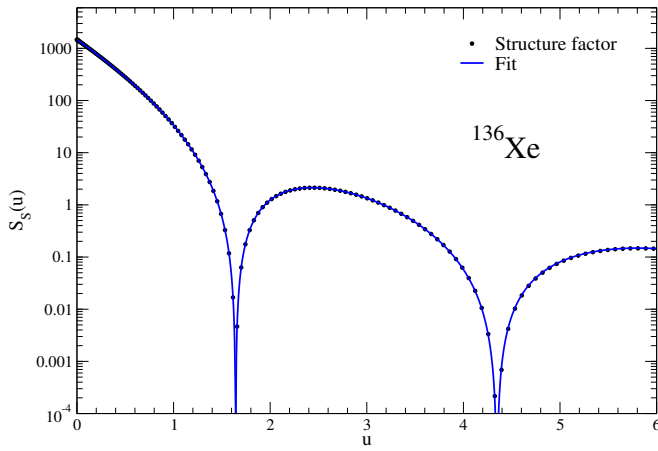


FIG. 13. (color online). Same as Fig. 6 but for  $^{136}\text{Xe}$ .

independent:

$$S_S(0) = A^2 c_0^2 \frac{2J+1}{4\pi}. \quad (9)$$

This reflects the well-known coherence of the contributions of all  $A$  nucleons in SI scattering. Consequently, near  $u = 0$  the spin-averaged structure factors are essentially identical for all xenon isotopes, apart from small variations in  $A^2$ .

Because of angular momentum coupling, only  $L = 0$  multipoles contribute to the structure factors of the even-mass isotopes. As discussed in Sec. II, parity and time reversal constrain the multipoles to even  $L$  for elastic scattering, so that for  $^{129}\text{Xe}$  only  $L = 0$ , and for  $^{131}\text{Xe}$  only  $L = 0, 2$  contribute. For the latter isotope, we show in Fig. 10 the separate contributions from  $L = 0$  and  $L = 2$  multipoles. At low momentum transfers, which is the most important region for experiment, the  $L = 0$  multipole is dominant, because coherence is lost for  $L > 0$  multipoles. Only near the minima of the  $L = 0$  multipole at  $u \sim 1.7$  and  $u \sim 4.4$  is the  $L = 2$  multipole

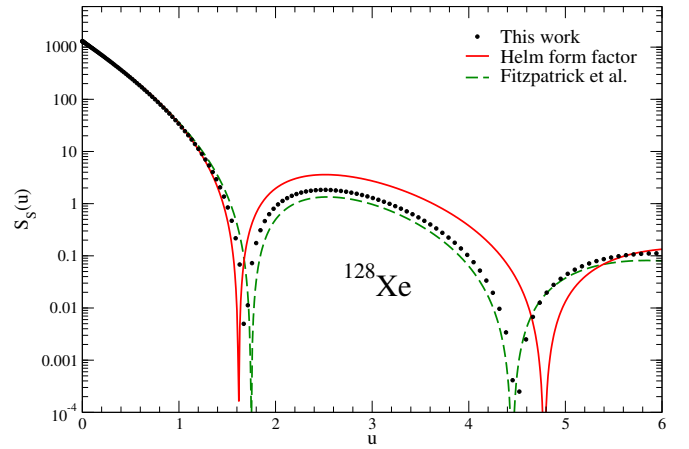


FIG. 14. (color online). Structure factor  $S_S(u)$  for  $^{128}\text{Xe}$  (this work, black dots) in comparison to the Helm form factor (solid red line) [25] and to the structure factor from Fitzpatrick *et al.* (dashed green line) [15].

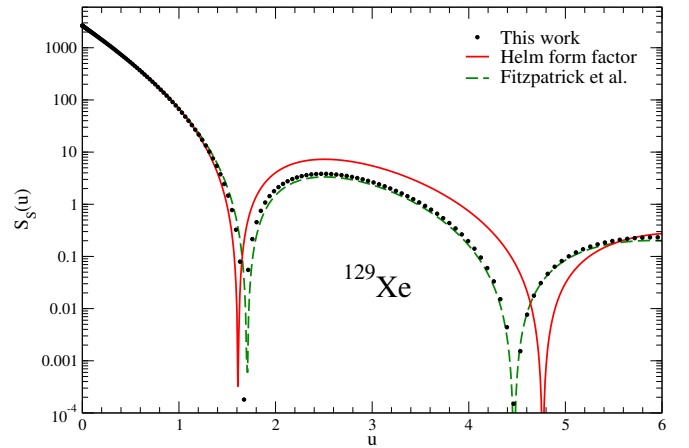


FIG. 15. (color online). Same as Fig. 14 but for  $^{129}\text{Xe}$ .

relevant, but the structure factor at these  $u$  values is suppressed with respect to  $S_S(0)$  by over four and six orders of magnitude, respectively.

Finally, we list in Table II the coefficients of the fits performed to reproduce the calculated structure factors for each isotope.

## V. COMPARISON TO HELM FORM FACTORS AND OTHER CALCULATIONS

In experimental SI WIMP scattering analyses the standard structure factor used to set limits on WIMP-nucleon cross sections is based on the Helm form factor [25]. This phenomenological form factor is not obtained from a detailed nuclear structure calculation, but is based on the Fourier transform of a nuclear density model, assumed to be constant with Gaussian surface. The corresponding

TABLE II. Spin/parity  $J^\Pi$ , harmonic-oscillator length  $b$ , and fit coefficients for the structure factors  $S_S(u)$  corresponding to  $S_S(u) = \frac{2J+1}{4\pi} e^{-u} (A + \sum_{i=1}^5 c_i u^i)^2$  for all stable xenon isotopes except  $^{131}\text{Xe}$  <sup>a</sup>, with  $u = q^2 b^2/2$ . The fit function corresponds to the analytical solution given in Refs. [26, 27].

Isotope	$^{128}\text{Xe}$	$^{129}\text{Xe}$	$^{130}\text{Xe}$	$^{131}\text{Xe}$ <sup>a</sup>	$^{132}\text{Xe}$	$^{134}\text{Xe}$	$^{136}\text{Xe}$
$J^\Pi$	$0^+$	$1/2^+$	$0^+$	$3/2^+$	$0^+$	$0^+$	$0^+$
$b$ (fm)	2.2827	2.2853	2.2879	2.2905	2.2930	2.2981	2.3031
$c_1$	-126.477	-128.119	-129.762	-131.284	-132.841	-135.861	-138.793
$c_2$	35.8755	36.5224	37.2824	37.9093	38.4859	39.6999	40.9232
$c_3$	-3.71573	-3.8279	-3.94541	-4.05914	-4.08455	-4.2619	-4.43581
$c_4$	0.138943	0.152667	0.158662	0.172425	0.153298	0.163642	0.169986
$c_5$	-0.00188269	-0.00287012	-0.00288539	-0.00386294	-0.0013897	-0.00164356	-0.00148137

<sup>a</sup> For  $^{131}\text{Xe}$  the fit function is given by  $S_S(u) = \frac{2J+1}{4\pi} e^{-u} [(A + \sum_{i=1}^5 c_i u^i)^2 + (\sum_{i=1}^5 d_i u^i)^2]$  with the additional fit coefficients:  $d_1 = 2.17510$ ,  $d_2 = -1.25401$ ,  $d_3 = 0.214780$ ,  $d_4 = -0.0111863$ , and  $d_5 = 9.21915 \cdot 10^{-5}$ .

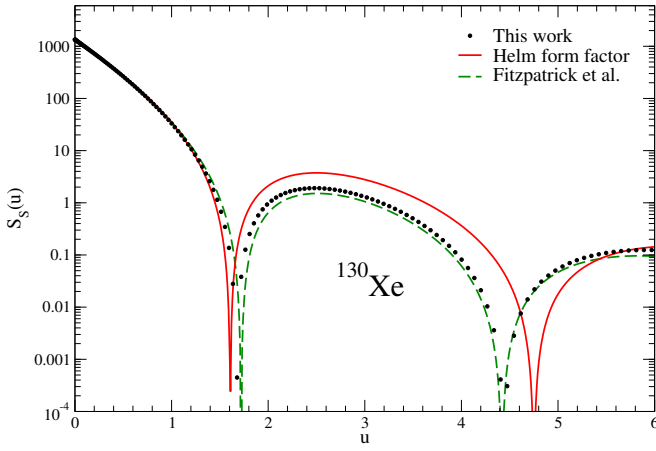


FIG. 16. (color online). Same as Fig. 14 but for  $^{130}\text{Xe}$ .

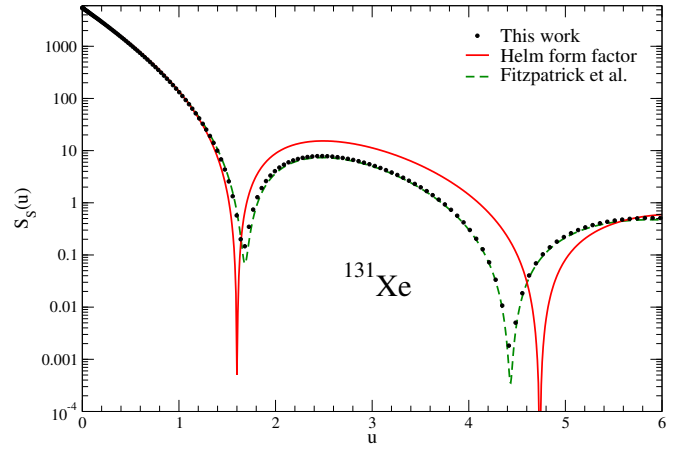


FIG. 17. (color online). Same as Fig. 14 but for  $^{131}\text{Xe}$ .

Helm structure factor has a simple analytical expression in terms of the nuclear radius  $r_n$  and surface thickness  $s$ :

$$S_S^{\text{Helm}}(q) = S_S(0) \left( \frac{3j_1(qr_n)}{qr_n} \right)^2 e^{-(qs)^2}. \quad (10)$$

The following parameterization is commonly used,  $r_n^2 = c^2 + \frac{7}{3}\pi^2 a^2 - 5s^2$ , with  $c = (1.23A^{1/3} - 0.60)$  fm,  $a = 0.52$  fm, and  $s = 1$  fm [25].

In Figs. 14–20, we compare the results for the structure factors presented in Sec. IV to the phenomenological Helm form factors given by Eq. (10). At low momentum transfers (and considering one-body currents only) the agreement is very good for all xenon isotopes. This validates the present use of Helm form factors in experimental SI analyses. Similar agreement is expected for other nuclei considered for WIMP-nucleus scattering.

The first minimum in  $S_S(u)$ , whose location is set by the nuclear radius, lies very close in our calculations and the Helm form factors. At higher momentum transfers small differences start to arise. The Helm form factors

lie somewhat above our calculations and have the second minimum at larger momentum transfers. We attribute these minor differences to the simple assumptions in the Helm form factors.

Figures 14–20 also compare our results to the structure factors calculated by Fitzpatrick *et al.* [15]. These shell-model calculations have been performed in the same valence space as in our work, but use an older nuclear interaction and restrict the configurations more severely than in our case (e.g., only  $^{134}\text{Xe}$  and  $^{136}\text{Xe}$  could be calculated in the full valence space). Nevertheless, the agreement between the structure factors of Ref. [15] and our present calculations is very good up to high momentum transfers. This shows that at this level SI WIMP scattering is not very sensitive to nuclear structure details of the isotopes involved. This conclusion was also reached for even-even nuclei based on Hartree-Fock calculations [28].

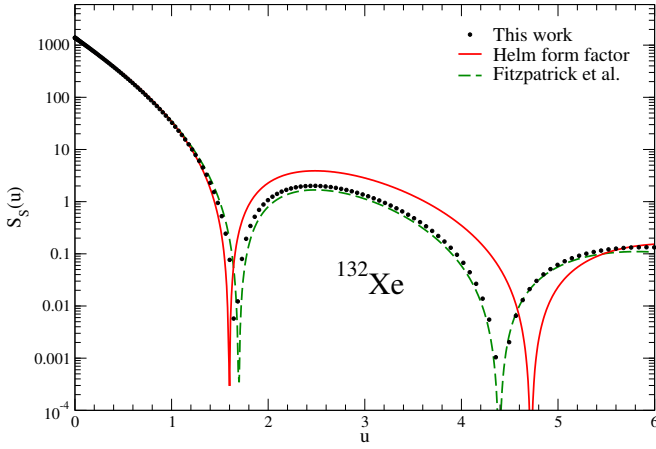


FIG. 18. (color online). Same as Fig. 14 but for  $^{132}\text{Xe}$ .

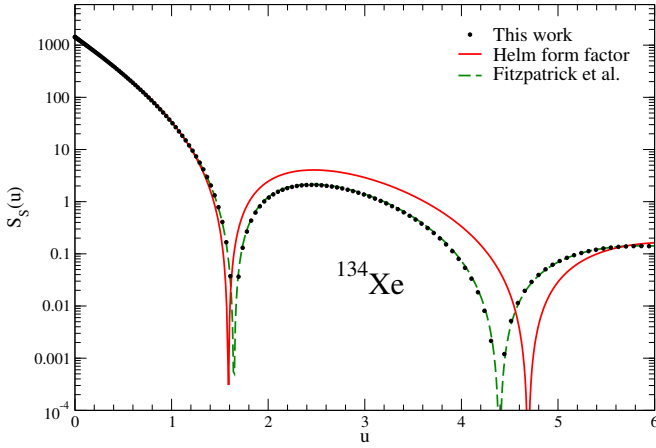


FIG. 19. (color online). Same as Fig. 14 but for  $^{134}\text{Xe}$ .

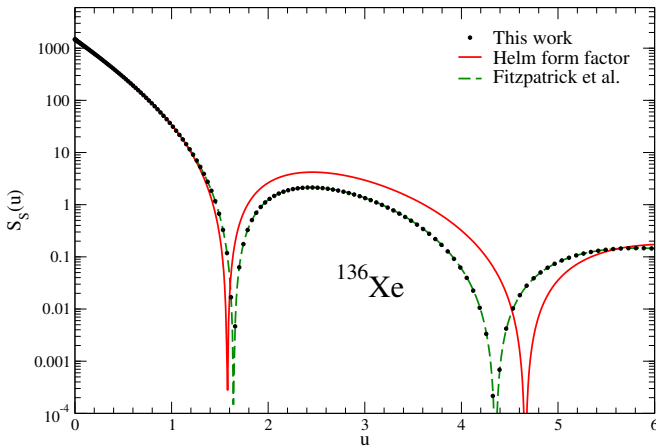


FIG. 20. (color online). Same as Fig. 14 but for  $^{136}\text{Xe}$ .

### A. Comparison for spin-dependent WIMP scattering

The interaction of WIMPs with nuclei can be also SD reflecting the coupling of the spin of the WIMP to nucleons. The even-mass xenon isotopes are practically insensitive to SD scattering due to their  $J = 0$  ground state, so that only the odd-mass xenon isotopes  $^{129}\text{Xe}$  and  $^{131}\text{Xe}$  are relevant. In previous work [11, 12], we have calculated SD structure factors for xenon, also including two-body currents in chiral effective field theory. To complete the study of WIMP scattering off xenon, we also compare these calculations to the results obtained by Fitzpatrick *et al.* in Ref. [15]. This provides a test of the calculations and explores the sensitivity of SD WIMP scattering to nuclear structure.

The SD structure factor is naturally decomposed in terms of the isospin couplings  $(a_0 + a_1\tau_3)/2$ . However, experimental results are commonly presented in terms of “neutron-only” ( $a_0 = -a_1 = 1$ ) and “proton-only” ( $a_0 = a_1 = 1$ ) structure factors  $S_n(u)$  and  $S_p(u)$ , because these coupling combinations are more sensitive to neutrons and protons, respectively. For vanishing momentum transfer,  $q = 0$  ( $u = 0$ ), and considering only one-body currents, the SD “neutron-only” and “proton-only” structure factors are proportional to the square of the expectation values of the neutron and proton spins [14]. These are given for both calculations in Table III. Because xenon has an even proton number,  $\langle S_n \rangle \gg \langle S_p \rangle$ , the “neutron-only” structure factor dominates over the “proton-only” one.

This hierarchy of “neutron-only” versus “proton-only” structure factors manifests itself in Figs. 21 and 22, where we show the calculated SD structure factors for  $^{129}\text{Xe}$  and  $^{131}\text{Xe}$ . Note that the absolute scale of the SD structure factors is  $\sim 10^{-4}$  smaller than for SI scattering, because in the SD case, due to pairing, the contributions from different nucleons do not add coherently.

In Refs. [11, 12], we included one- and two-body currents in the WIMP-nucleon interaction Lagrangian. However, for a direct comparison, Figs. 21 and 22 restrict the results to the one-body level, even though two-body currents are important because they reduce the “neutron-only” structure factors by about 20% for xenon, and significantly enhance the “proton-only” structure factors at

TABLE III. Proton/neutron spin expectation values  $\langle S_{p/n} \rangle$  for  $^{129}\text{Xe}$  and  $^{131}\text{Xe}$ . Results are shown for the calculations of Klos *et al.* [12], which use the same valence space and nuclear interactions as in this work, and of Fitzpatrick *et al.* [15].

	$^{129}\text{Xe}$		$^{131}\text{Xe}$	
	$\langle S_p \rangle$	$\langle S_n \rangle$	$\langle S_p \rangle$	$\langle S_n \rangle$
Klos <i>et al.</i> [12]	0.010	0.329	-0.009	-0.272
Fitzpatrick <i>et al.</i> [15]	0.007	0.248	-0.005	-0.199

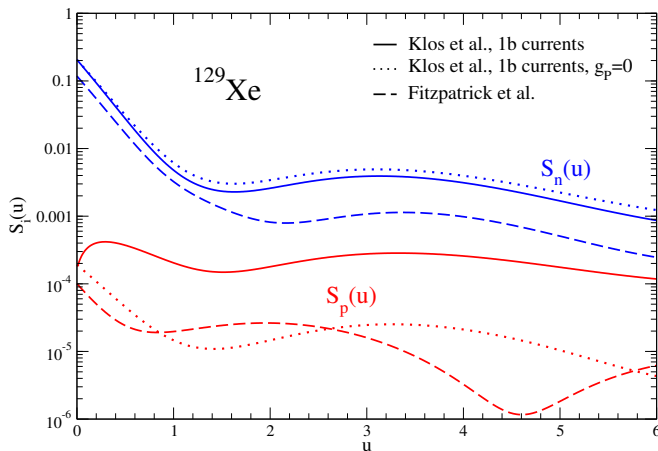


FIG. 21. (color online). Comparison of “neutron-only”  $S_n(u)$  (blue) and “proton-only”  $S_p(u)$  (red lines) spin-dependent structure factors for  $^{129}\text{Xe}$ : results are shown from Klos *et al.* [12] at the one-body (1b) current level with/without pseudoscalar ( $g_P$ ) contributions (solid/dotted lines) and from Fitzpatrick *et al.* [15] (dashed lines).

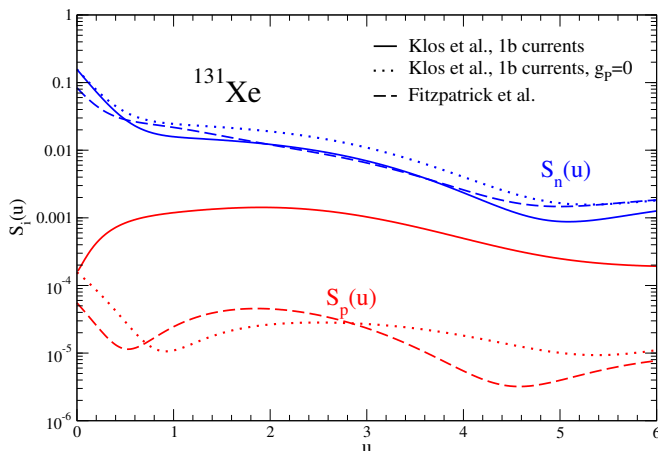


FIG. 22. (color online). Same as Fig. 21 but for  $^{131}\text{Xe}$ .

small momentum transfers [11, 12]. In addition to the structure factors calculated with the full one-body currents, Fig. 21 and Fig. 22 also show results without the pseudoscalar contributions ( $g_P = 0$ ). This choice can be directly compared to the operator used by Fitzpatrick *et al.* [15], because the pseudoscalar contributions are considered as an independent response [15].

A comparison of the different calculations in Figs. 21 and 22 shows larger differences than for SI scattering. This is because the SD case is more sensitive to nuclear structure details. At  $u = 0$  this difference can be traced to the larger spin expectation value obtained in Klos *et al.* [12] (see Table III), which is a modest 1.3 times larger than in Fitzpatrick *et al.* [15] for both isotopes. The difference is due to the more recent nuclear interaction

used with less truncations, and also explains why this “neutron-only” response is larger for any  $u$  value. Figures 21 and 22 also show that, for finite momentum transfer, the pseudoscalar contributions enhance the “proton-only” structure factor by about one order of magnitude. This is because when this isovector term is included, neutrons, which carry most of the spin in xenon, can contribute to the “proton-only” response. Because the relative strength of axial and pseudoscalar contributions in the Fitzpatrick *et al.* calculation [15] are taken to be a ratio of independent couplings, we compare the two calculations in the limit where the pseudoscalar coupling is turned off. In this limit, the results are comparable at higher momentum transfers and the differences are similar as for the neutron-only case.

We emphasize that the two shell-model calculations agree in the sign and magnitude of the matrix element ratios  $\langle \mathbf{S}_p \rangle / \langle \mathbf{S}_n \rangle \sim 0.03$  for both isotopes, so that the proton amplitude is about 3% of the total. Moreover, the agreement between structure factors in the physically relevant region  $u \lesssim 1$  is better than at high-momentum transfers, where other corrections not included in these calculations will be relevant. This shows that the uncertainties in the structure factors are modest, so that they should not limit the extraction of dark matter information from direct detection experiments (see also the conclusions of Ref. [29]).

## VI. SPIN-INDEPENDENT VS. SPIN-DEPENDENT INELASTIC SCATTERING

The xenon isotopes  $^{129}\text{Xe}$  and  $^{131}\text{Xe}$  have  $J_f = 3/2^+$  and  $J_f = 1/2^+$  low-lying excited states at 39.6 keV and 80.2 keV, respectively, that could be excited in inelastic WIMP scattering. In Ref. [13] we showed that for these isotopes, at the momentum transfers kinematically allowed for inelastic scattering (corresponding to  $u \sim 1$ ), the SD elastic and inelastic structure factors are comparable, and the inelastic maxima are suppressed by only a factor 10 compared to the elastic case. This opens the door to the detection of SD inelastic WIMP scattering off xenon. Note that elastic scattering is always dominant because of its maximum at  $q = 0$  and more favorable kinematics.

Figures 23 and 24 show the calculated structure factors for SI inelastic scattering to the lowest excited state in  $^{129}\text{Xe}$  and  $^{131}\text{Xe}$ . Angular momentum and parity considerations limit the multipole contributions to  $L = 2$  in both cases. For SI inelastic scattering, the contributions from different nucleons do not add coherently, and the structure factors are suppressed by several orders of magnitude with respect to the elastic case. At the kinematically allowed region for inelastic scattering around  $u \sim 1$ , the suppression is about a factor  $2 \cdot 10^{-3}$  for  $^{129}\text{Xe}$  and  $10^{-4}$  for  $^{131}\text{Xe}$ . When comparing the global maxima for elastic and inelastic scattering, the suppression is even stronger, by factors of about  $10^{-4}$  and  $5 \cdot 10^{-5}$ ,

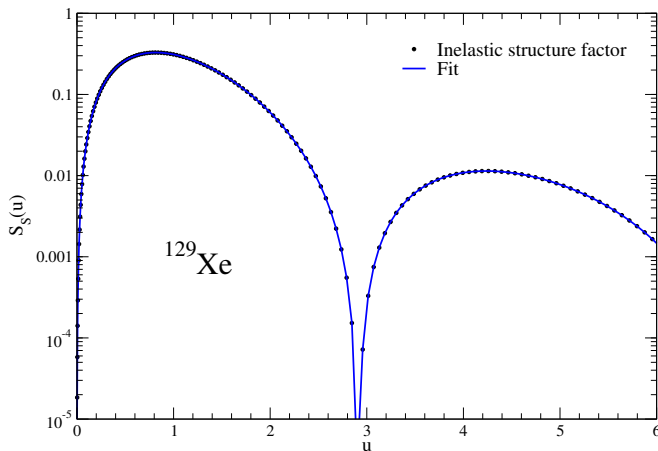


FIG. 23. (color online). Spin-independent inelastic structure factor for  $^{129}\text{Xe}$  (black dots), from the  $J_i = 1/2^+$  ground state to the  $J_f = 3/2^+$  excited state at 39.6 keV, with a fit (solid blue line) given in Table IV.

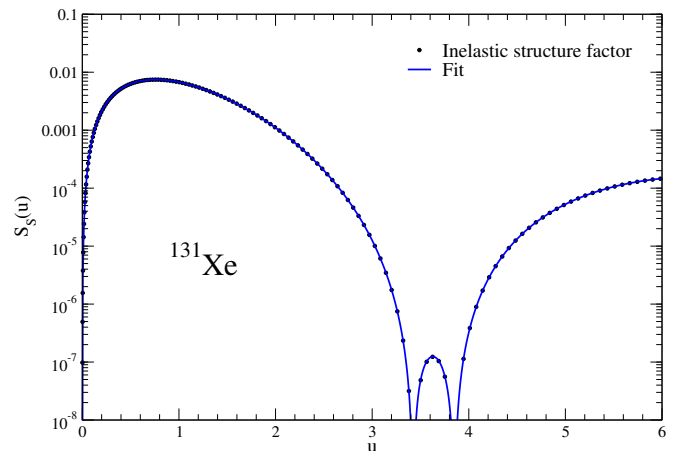


FIG. 24. (color online). Spin-independent inelastic structure factor for  $^{131}\text{Xe}$  (black dots), from the  $J_i = 3/2^+$  ground state to the  $J_f = 1/2^+$  excited state at 80.2 keV, with a fit (solid blue line) given in Table IV.

respectively, in stark contrast to SD scattering.

TABLE IV. Fit coefficients for the inelastic structure factors  $S_S(u)$  corresponding to  $S_S(u) = \frac{2J_i+1}{4\pi} e^{-u} (\sum_{i=1}^5 d_i u^i)^2$  for  $^{129}\text{Xe}$  and  $^{131}\text{Xe}$ , with  $u = q^2 b^2/2$  and  $J_i = 1/2^+$  and  $J_i = 3/2^+$ , respectively. The fit function corresponds to the analytical solution given in Refs. [26, 27]. The harmonic-oscillator lengths  $b$  are as in Table II.

Isotope	$^{129}\text{Xe}$	$^{131}\text{Xe}$
$d_1$	4.46850	0.515046
$d_2$	-2.54918	-0.341605
$d_3$	0.406162	0.0707621
$d_4$	-0.0206094	-0.00436258
$d_5$	0.000258314	$9.81102 \cdot 10^{-7}$

This explicitly confirms that inelastic scattering can discriminate between SI and SD interactions, as detection of the inelastic channel would point to a SD WIMP-nucleus coupling [13]. Finally, the fit coefficients for the SI inelastic structure factors for  $^{129}\text{Xe}$  and  $^{131}\text{Xe}$  are listed in Table IV.

## VII. SUMMARY

We have studied SI WIMP scattering off xenon using the leading one-body scalar currents. Our nuclear structure calculations are based on state-of-the-art shell-model calculations in the largest valence spaces with interactions that have been tested against spectroscopy and decay studies. In particular, the spectra of all relevant xenon isotopes are very well reproduced.

Based on these nuclear interactions, we have calculated the structure factors for the xenon isotopes. These present the consistent calculations to the SD results in Refs. [12], providing fits for all structure factors. For the momentum transfers relevant to direct detection experiments,  $u \lesssim 1$ , the calculated structure factors are in very good agreement with the phenomenological Helm form factors used to give experimental limits for dark matter detection. This shows that the presently extracted limits from SI [8, 9] and SD [30] interactions off xenon are consistent in the underlying nuclear structure used for the analysis.

In addition we have compared our results for the structure factors to the shell-model calculations of Fitzpatrick *et al.* [15], which have been performed with more truncations and older nuclear interactions. However, because SI scattering is sensitive to the nucleon density distribution, both calculations agree well. In particular, for  $u \lesssim 1$ , the agreement is excellent. This shows that the spin-independent structure factor is not very sensitive to details in nuclear interactions. However, we emphasize that additional contributions are expected from two-body currents [16, 17].

In contrast, for SD interactions, even at the one-body level, there are larger differences between the results of Klos *et al.* [12], which use the same nuclear interactions as in this work, and those of Fitzpatrick *et al.* [15]. These differences are mostly due to the different spin expectation values at  $u = 0$ . However, these differences are modest and should not limit the extraction of dark matter information from direct detection experiments. Efforts to further reduce the uncertainties based on nuclear structure input are underway.

Finally, we have calculated the structure factors for SI inelastic scattering for the odd-mass xenon isotopes  $^{129}\text{Xe}$  and  $^{131}\text{Xe}$ . These have low-lying excited states that can

be accessed by WIMP scattering [13]. As expected, the inelastic response is suppressed by  $\sim 10^{-4}$  compared to coherent elastic scattering. Therefore, the detection of inelastic scattering is able to discriminate clearly between SI and SD scattering, because the SD inelastic structure factor, while suppressed relative to elastic scattering at  $u = 0$ , becomes comparable for  $u \sim 1$ , where the inelastic response is suppressed only by a factor 10 with respect to the elastic maximum. This demonstrates how using nuclear properties will be important for decoding the information from dark matter signals.

## ACKNOWLEDGMENTS

We thank M. Hoferichter for discussions. This work was supported by ARCHES, the DFG through Grant No. SFB 634, the ERC Grant No. 307986 STRONGINT, the Helmholtz Alliance Program of the Helmholtz Association, contract HA216/EMMI “Extremes of Density and Temperature: Cosmic Matter in the Laboratory”, and by the US Department of Energy under Contracts DE-SC00046548 and DE-AC02-98CH10886. W. H. thanks the Alexander von Humboldt Foundation for support.

- 
- [1] J. L. Feng, *Annu. Rev. Astron. Astrophys.* **48**, 495 (2010).
  - [2] G. Bertone, *Particle Dark Matter: Observations, Models and Searches* (Cambridge University Press, Cambridge, England, 2010).
  - [3] L. Baudis, *Phys. Dark Univ.* **1**, 94 (2012).
  - [4] Z. Ahmed *et al.* (CDMS II Collaboration), *Phys. Rev. Lett.* **106**, 131302 (2011).
  - [5] E. Armengaud *et al.* (Edelweiss II Collaboration), *Phys. Lett. B* **702**, 329 (2011).
  - [6] M. Felizardo *et al.* (SIMPLE Collaboration), *Phys. Rev. Lett.* **108**, 201302 (2012).
  - [7] D. Akimov *et al.* (ZEPLIN-III Collaboration), *Phys. Lett. B* **709**, 14 (2012).
  - [8] E. Aprile *et al.* (XENON100 Collaboration), *Phys. Rev. Lett.* **109**, 181301 (2012).
  - [9] D. S. Akerib *et al.* (LUX Collaboration), *Phys. Rev. Lett.* **112**, 091303 (2014).
  - [10] J. R. Ellis, R. A. Flores, and J. D. Lewin, *Phys. Lett. B* **212**, 375 (1988).
  - [11] J. Menéndez, D. Gazit, and A. Schwenk, *Phys. Rev. D* **86**, 103511 (2012).
  - [12] P. Klos, J. Menéndez, D. Gazit, and A. Schwenk, *Phys. Rev. D* **88**, 083516 (2013).
  - [13] L. Baudis, G. Kessler, P. Klos, R. F. Lang, J. Menéndez, S. Reichard, and A. Schwenk, *Phys. Rev. D* **88**, 115014 (2013).
  - [14] J. Engel, S. Pittel, and P. Vogel, *Int. J. Mod. Phys. E* **01**, 1 (1992).
  - [15] A. L. Fitzpatrick, W. Haxton, E. Katz, N. Lubbers, and Y. Xu, *JCAP* **1302**, 004 (2013).
  - [16] G. Prézeau, A. Kurylov, M. Kamionkowski and P. Vogel, *Phys. Rev. Lett.* **91**, 231301 (2003).
  - [17] V. Cirigliano, M. L. Graesser, and G. Ovanessian, *JHEP* **1210**, 025 (2012).
  - [18] S. R. Beane, S. D. Cohen, W. Detmold, H.-W. Lin, and M. J. Savage, *Phys. Rev. D* **89**, 074505 (2014).
  - [19] J. D. Walecka, *Theoretical Nuclear and Subnuclear Physics* (Oxford University Press, New York, 1995).
  - [20] E. Caurier, J. Menéndez, F. Nowacki, and A. Poves, *Phys. Rev. Lett.* **100**, 052503 (2008).
  - [21] J. Menéndez, A. Poves, E. Caurier, and F. Nowacki, *Nucl. Phys. A* **818**, 139 (2009).
  - [22] E. Caurier and F. Nowacki, *Acta Phys. Pol. B* **30**, 705 (1999).
  - [23] E. Caurier, G. Martínez-Pinedo, F. Nowacki, A. Poves, and A. P. Zuker, *Rev. Mod. Phys.* **77**, 427 (2005).
  - [24] <http://www.nndc.bnl.gov/ensdf/>.
  - [25] J. D. Lewin and P. F. Smith, *Astropart. Phys.* **6**, 87 (1996).
  - [26] T. W. Donnelly and W. C. Haxton, *At. Nucl. Data Tables* **23**, 103 (1979).
  - [27] W. C. Haxton and C. Lunardini, *Comput. Phys. Commun.* **179**, 345 (2008).
  - [28] G. Co’, V. De Donno, M. Anguiano, and A. M. Lallena, *J. Cosmol. Astropart. Phys.* **11** (2012) 010.
  - [29] D. G. Cerdeño, M. Fornasa, J. H. Huh, and M. Peiró, *Phys. Rev. D* **87**, 023512 (2013).
  - [30] E. Aprile *et al.* (XENON100 Collaboration), *Phys. Rev. Lett.* **111**, 021301 (2013).